Immersed Boundary Simulations of Aeroacoustics Phenomena in Solid Rocket Motors

Matteo Cimini⋆, Fulvio Stella⋆, Enrico Cavallini ††, Andrea Di Mascio ⋆⋆, Agostino Neri ⋆⋆⋆,
Emanuele Martelli† and Matteo Bernardini⋆

⋆Sapienza Università di Roma
Via Eudossiana 18, Roma, Italy

††Agenzia Spaziale Italiana
Via del Politecnico snc, Roma, Italy

⋆⋆ Università degli Studi dell'Aquila
Via Gronchi 18, L'Aquila, Italy

⋆⋆⋆ European Space Agency
Frascati, Italy

†Università dgli Studi della Campania L. Vanvitelli
Via Roma 29, Aversa, Italy

Abstract

The combustion of heterogeneus solid propellants are characterized by velocity fluctuations which have a fundamental effect on the turbulence development and on the onset of aeroacoustic instabilities. In this work, following open literature, we propose a parametric study to develop a specific mass-injection boundary condition able to account for such fluctuations. This new propellant boundary condition is implemented in a advanced flow solver which adopt the immersed boundary methodology to deal with complex geometries and applied to a real rocket motor inspired by the second stage of the european VEGA launcher. The numerical results show that it is possible to tune the model in order to correctly reproduce the amplitude and the main frequency of the pressure oscillations which develop inside the combustion chamber.

1. Introduction

This work aims at investigating the flow dynamics in solid rocket motors (SRMs), which are still of a great interest for space launchers. The internal ballistics of SRMs is generally characterized by the interaction of the hydrodynamic instabilities that develop from shear layers in different parts of the motor and the acoustic resonant modes of the combustion chamber. This possible coupling can trigger pressure oscillations, which are able to even jeopardize the motor structures, the thrust vector control system and the payload integrity. In this work we want to reproduce the internal flow in a rocket geometry which resembles the second stage of European Space Agency (ESA) launcher Vega-C, named Zefiro-40. The interest for this motor stems from the activation of internal pressure oscillation recorded during the experiments. In particular, seventeen seconds after the ignition, the pressure probe on the head of the motor records an oscillation around the average non-dimensional value of about 0.897: the non-dimensional amplitude of the oscillation is approximately 0.0016, and the primary oscillation non-dimensional frequency is ∼ 0.385.

The problem of pressure oscillations in SRMs has received considerable attention in the last decades. Given the intrinsic limitation of simplified methods to predict instabilities in SRMs, several studies have been carried out to characterize the flow behavior in the chamber and assess the capability of full numerical simulations to predict vortex shedding and pressure oscillations. Most of the numerical works available in literature are based on quasi-1D models or 2D simulations, whereas only recently 3D high-fidelity numerical simulations have appeared. The latter study, clearly highlighted the importance of accurately simulating the turbulent flow field in the combustion chamber in order to correctly predict the level of pressure oscillations [1]. Another important modeling issue is related to the burning-grain boundary condition. Indeed, following the work of Gallier and Plaud [3] and Massa et al [6] among others, it is well known that composite propellants are heterogeneous at microscale and their combustion originate local fluctuations of gas velocity which are space- and time-correlated. One of the main objective of this work is to correclty model the fluctuation characteristics in order to increase the reliability of simulations of the turbulent flow instabilities. In

addition, we propose to adopt the immersed boundary method to perform high-fidelity large eddy simulations of the internal ballistics of Zefiro 40. This technique offers several advantages with respect to standard method based on body-fitted grids and allows to easy handle complex configurations.

2. Numerical results: Zefiro–40 like geometry

In order to describe the internal flow in the rocket combustion chamber, we performed a series of numerical simulations using the immersed boundary approach, as described in Di Mascio and Zaghi [2], on a simplified cylindrical geometry. To this purpose, a signed distance function locates the boundary of the flow field on a regular Cartesian mesh (see figure 1) and identifies internal points; we solve the discrete form of the compressible Navier–Stokes equations, whereas we extrapolate the solution on external points in order to enforce the proper boundary conditions on both the solid (adiabatic) walls and the burning grain, where mass inflow and flame temperature are assigned. On solid walls, we computed the tangential stress utilizing wall functions [9].
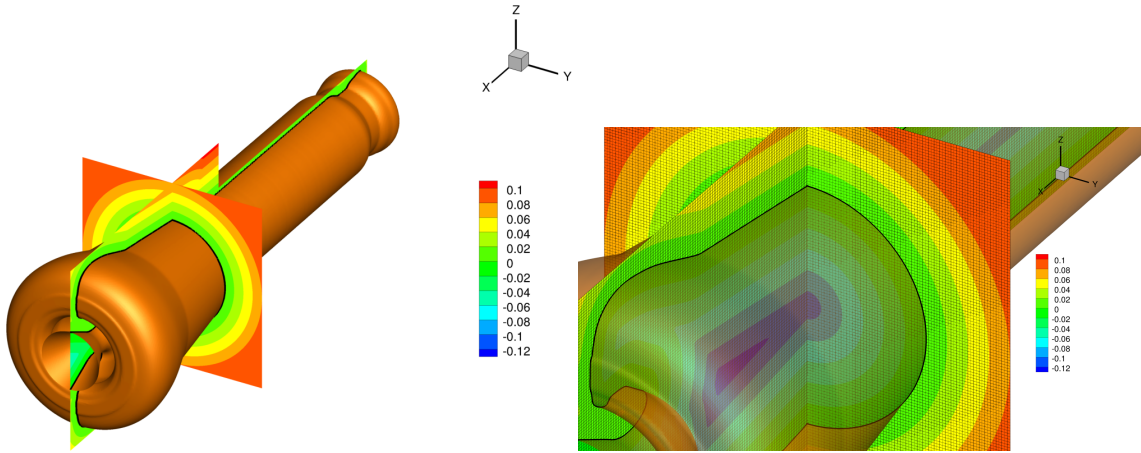

Figure 1: Geometry and grid

For space discretization, we used a seventh order Weighted Essentially non Oscillating (WENO) scheme (see Jiang et al. [5] and Gerolimos et al [4]) to discretize the equations via the flux splitting approach of Steger and Warming [8]. We used a third order TVD Runge–Kutta scheme for time discretization [5]. We applied the Detached Eddy Simulation described in Spalart et al. [7] to simulate turbulent fluctuations. As to the numerical set–up, the grid adopted in the simulation consists of $\sim$ 5.1 million cells, with a cell size of about 0.00265 (the distance between the head and the throat is the reference length). The time step is such that the Courant-Friedrichs-Lewy condition is constantly equal to 0.9.

We first computed the flow field at the nominal condition of the burning rate and flame temperature. Figure 2 reports the solution on a longitudinal cross-section in terms of Mach number and vorticity component normal to the plotted surface. The flow develops in a low subsonic regime (the Mach number M is below 0.05) in most of the chamber, reaching $M = 2.75$ at the nozzle discharge. An axisymmetric shear layer starting from the edge in the grain geometry appears; this structure seems to be very stable. Unlike the experimental observations, the flow simulation in the above conditions yields an almost steady flow, with oscillation amplitude below 10^{-5}.

The departure from the experimental observation is probably due to the grain inhomogeneity, which is always present in propellants. To replicate the observed pressure oscillations, we added a random perturbation to the boundary conditions on the burning grain. In a first attempt, we added a random perturbation to the grain's mass flow and temperature. The amplitude for the perturbation was equal to 50% of the nominal mass flow per unit area $\dot{m} = \rho u_n$; the resulting mass flow is

$$\dot{m}_r = \dot{m}\left(1 + r\right)$$

r being a random number such that $-0.5 < r < 0.5$ with a null average. The perturbation for the flame temperature T_f is a random fluctuation ΔT_f such that the variation of the internal energy on the boundary was of the same order of magnitude of the variation for the kinetic energy, i.e.

$$T_r = T_f + \Delta T_f = T_f + sign(r_t)\frac{(r_t u_n)^2}{2C_v} = T_f + r_t|r_t|\frac{u_n^2}{2C_v}$$

where r_t is another random number such that $-0.5 < r_t < 0.5$ and C_v is the specific heat at constant volume.
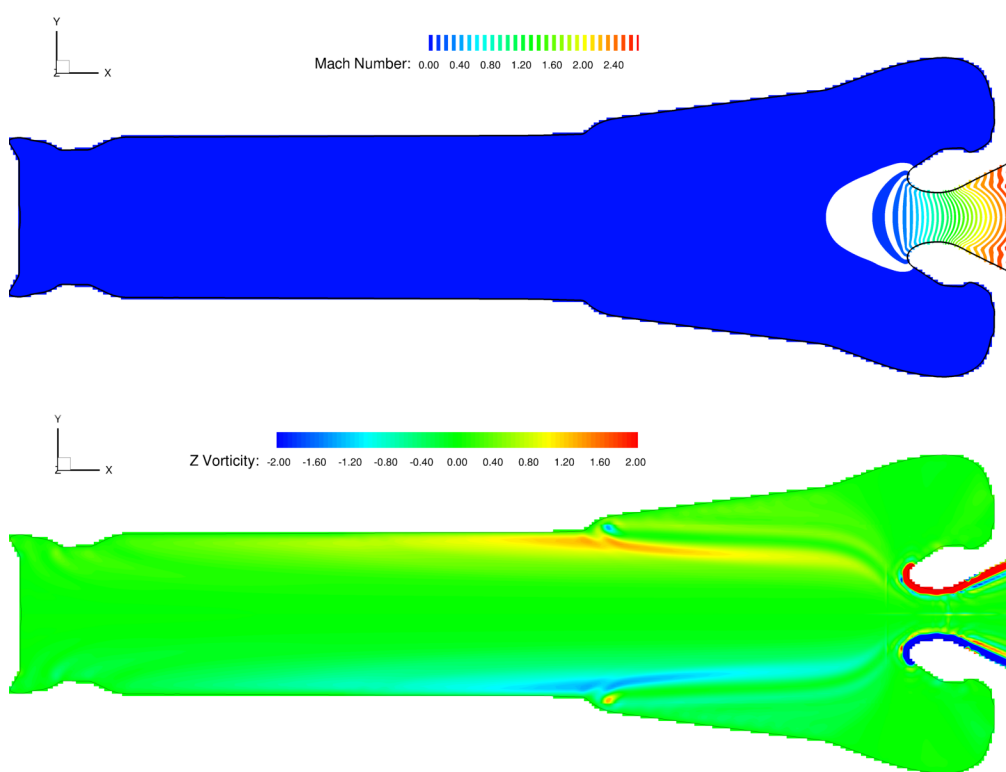
Figure 2: Reference solution (no perturbation). Top: Mach number distribution; bottom: z component of vorticity.

The result for this first attempt was completely unsatisfactory because the perturbation gave rise to relevant pressure fluctuation (around 0.002), but the spectrum for the head pressure revealed that all the energy content is around a non-dimensional frequency equal to 50, much higher than the observed frequency during the mission (see figure 3).
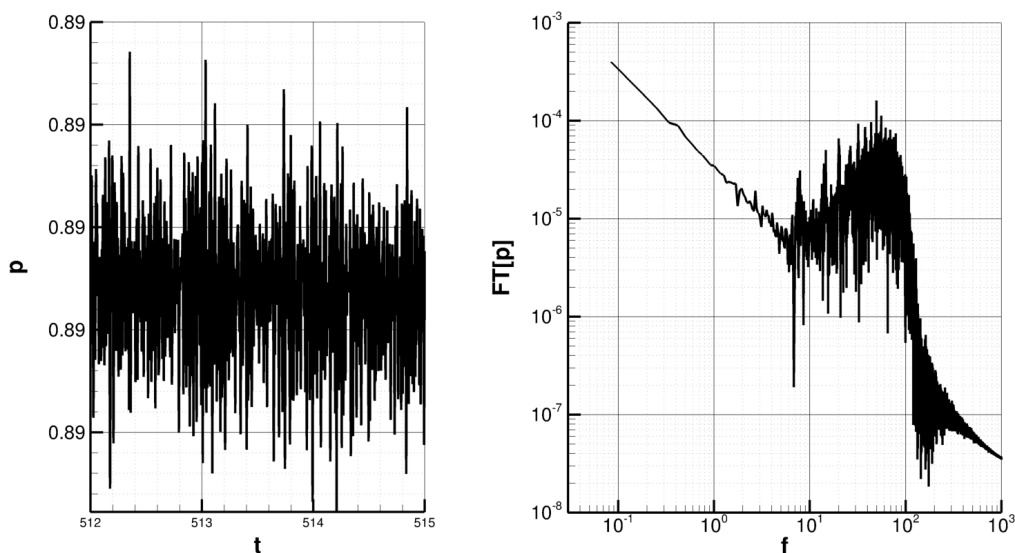
Figure 3: Time history (left) and Fourier transform(right) of the head pressure signal for a fully random perturbation.

On the other side, the investigation carried out in Massa et al. [6] revealed that above a heterogeneous propellant, the observed fluctuations of velocity and temperature are relevant (with peak values for the velocity perturbation up to 100% of the nominal value). More importantly, they observed that both velocity and temperature fields exhibit space and time correlations. Of course, these correlation scales depend on the type of propellant and its production process; nevertheless, they found that for realistic grains, the space correlation scale is always of the order of $1.9 \cdot 10^{-5}$ or smaller

and the time correlation scale is always between 0.2 and 0.6.

From the simulation point of view, the space correlation found in the cited paper is always much smaller than the cell size for realistic grids, and therefore it can not be resolved. On the contrary, the time scale is much larger than the numerical time step Δt: in the present simulations, for instance, for the chosen stability limits $\Delta t = O(2 \cdot 10^{-4})$ for the grid adopted. Consequently, we decided to repeat the simulations with an uncorrelated perturbation in space, whereas we investigated the effects of varying the time correlation.

In order to obtain the desired correlation characteristics, we proceeded as follows. First of all, we define the correlation function $R(\tau)$ from the convolution integral $C(\tau)$ as

$$R(\tau) = \frac{C(\tau)}{C(0)} \qquad \text{where} \qquad C(\tau) = \int_{-T_0/2}^{T_0/2} u(t)u(t+\tau)dt \qquad (1)$$

where T_0 is the observation period. Then, a random perturbation is generated for each point in space, which is kept constant for a time interval equal to the chosen correlation time. For instance, if we want a time correlation equal to 10^{-3}, the signal in time would look like the one reported in figure 4. With this form, the computed correlation function is reported in figure 5. As shown in the figures, the autocorrelation function is significantly different from zero only for
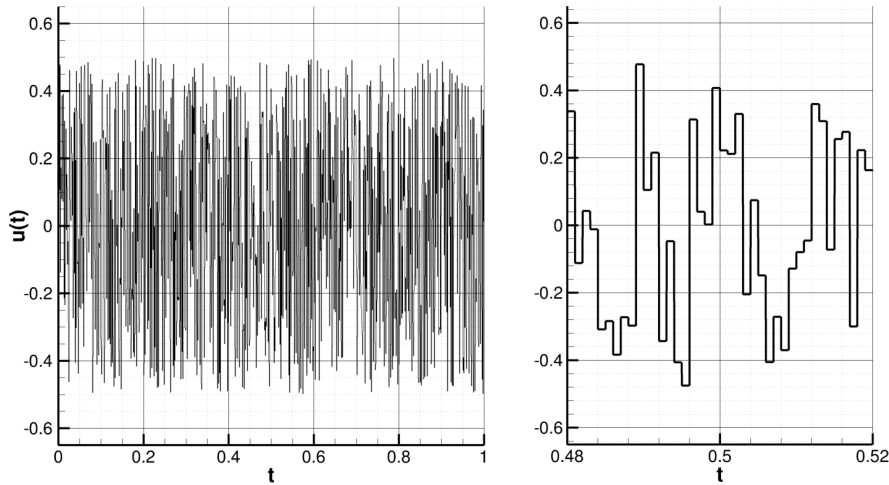

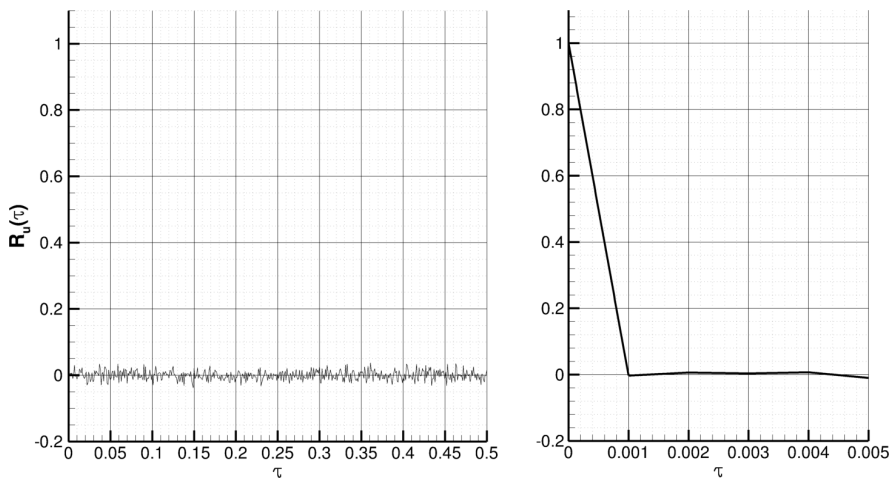Figure 4: Random signal $u(t)$. Left: global view for $0 < t < 1$; right: zoomed view

Figure 5: Autocorrelation function $R(\tau)$. Left: global view; right: zoomed view around $\tau = 0$

τ smaller than the chosen time scale, while is almost null elsewhere. Although the resulting function is much simpler than the actual one, in this way it is very easy to control the time correlation and remove the ambiguity arising from more complex signals.
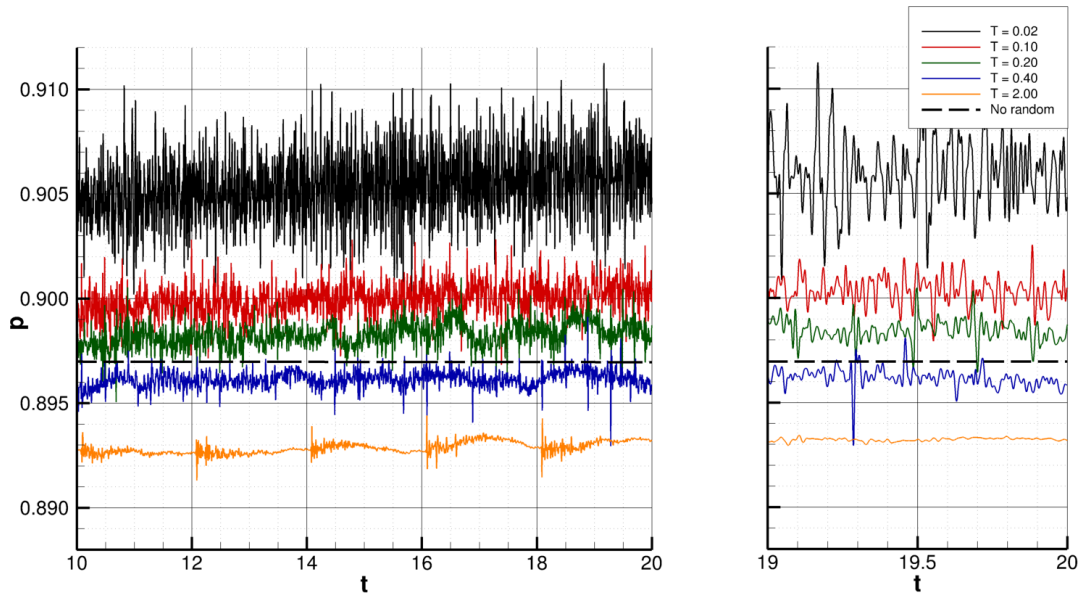
4

Figure 6: History of head pressure for random perturbations with different correlation times and amplitude = 50%. Left: global view; right: zoomed view.

The computed pressure signals recorded at the motor head are reported in figure 6, whereas a summary of the relation between the amplitude of pressure oscillation and the time correlation scale is shown in figure 7. The amplitude of pressure oscillation A, defined as

$$A = 2\sqrt{\frac{2}{T}\int_0^T (p - p_{ave})^2 dt}$$

where T is the observation interval and p_{ave} is the average pressure (we multiplied the standard root mean square by the factor $2\sqrt{2}$, so that the amplitude is equal to the difference between the maximum and the minimum for a pure sinusoidal oscillation). The plot shows that the response amplitude decreases with the time correlation scale.

Figure 8 shows the relation between the frequency with the largest energy content in the pressure spectrum $F(p)(\omega)$ and the correlation time. As can be seen, the dominant frequency in the spectrum is very high for short correlation times. On the contrary, when the time scale is between 0.2 and 2, the most energetic response always appears in a non-dimensional frequency range between 0.37 and .40. Figure 9 reports details of the head pressure spectrum; from the plots, it is clearly visible the rise of a dominant frequency around 0.40 for time scales between $\tau = 0.4$ and $\tau = 2$.

Figure 10 shows the instantaneous flow fields for different values of the time correlation in terms of the Z component of the vorticity on the plane $z = 0$. Note that the regular shear layer observed in the absence of perturbation breaks into vortices that are convected downstream, similarly to what happens in the flow field in other solid propellant rockets [1]; moreover, the original shear layer of the reference solution becomes hardly recognizable for the higher correlation time scales. At the same time, smaller and relatively regular vortices of increasing strength appear all along the cylindrical wall of the grain in the constant section portion of the propellant; these vortices are convected downstream by the bulk flow and are probably responsible for the unsteadiness and collapse of the shear layer emanating from the kink in the grain geometry.

As additional test cases, we also checked the effects of the perturbation amplitude on the response amplitude for a fixed correlation time $T = 0.4$. Figure 11 shows that, as expected, the oscillation amplitude grows with the amplitude of the exciting perturbation. Surprisingly, also the average head pressure strongly depends on it in a rather unexpected way (see figure 12). This last aspect will be the subject of the follow-up of the research.

3. Conclusions

In thsi work we have simulated a SRM geometry resembling the second stage of the VEGA-C launcher. A parametric analysis has been carried out in order to characterize the correct amplitude and correlation time of the fluctuations in the injection velocity field, originated by the combustion of heterogeneous propellants in a real motor. We verified that
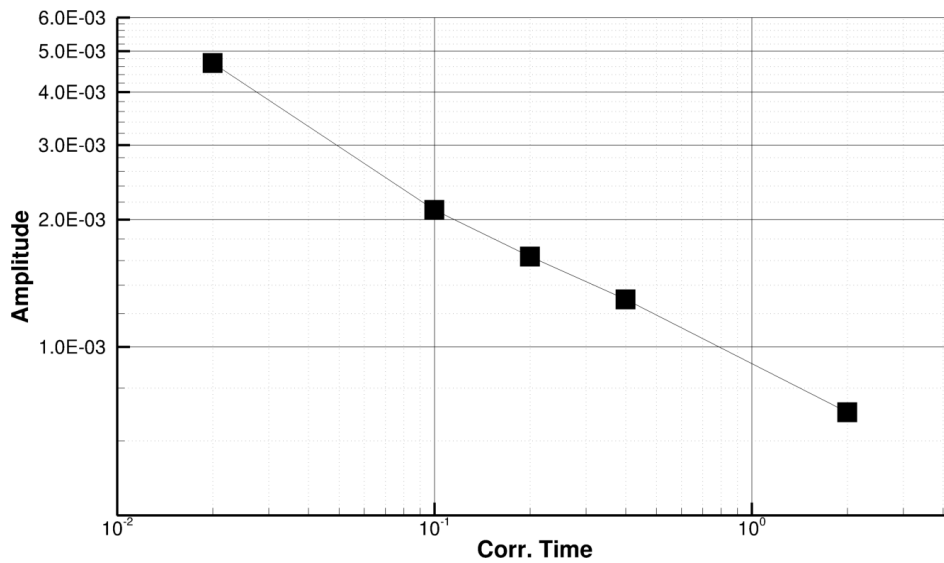
Figure 7: Amplitude of head pressure oscillation versus correlation times (in *s*) for a random perturbation amplitude of 50%.
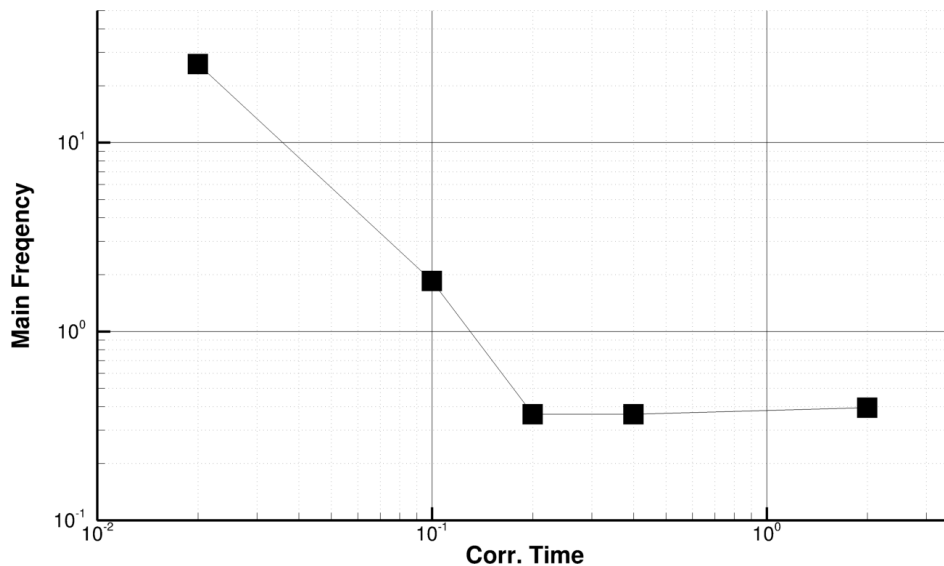

Figure 8: Dominant frequency of head pressure oscillation versus correlation times for a random perturbation amplitude of 50%.

it is possible to find a combination of intensity and correlation time able to reproduce the main frequency and amplitude of the pressure oscillation in the combustion chamber.

4. Acknowledgments

References

[1] M Bernardini, M Cimini, F Stella, E Cavallini, A Di Mascio, A Neri, and E Martelli. Large-eddy simulation of vortex shedding and pressure oscillations in solid rocket motors. *AIAA Journal*, 58(12):5191–5201, 2020.

[2] Andrea Di Mascio and Stefano Zaghi. An immersed boundary approach for high order weighted essentially non-oscillatory schemes. *Computers & Fluids*, 222:104931, 2021.
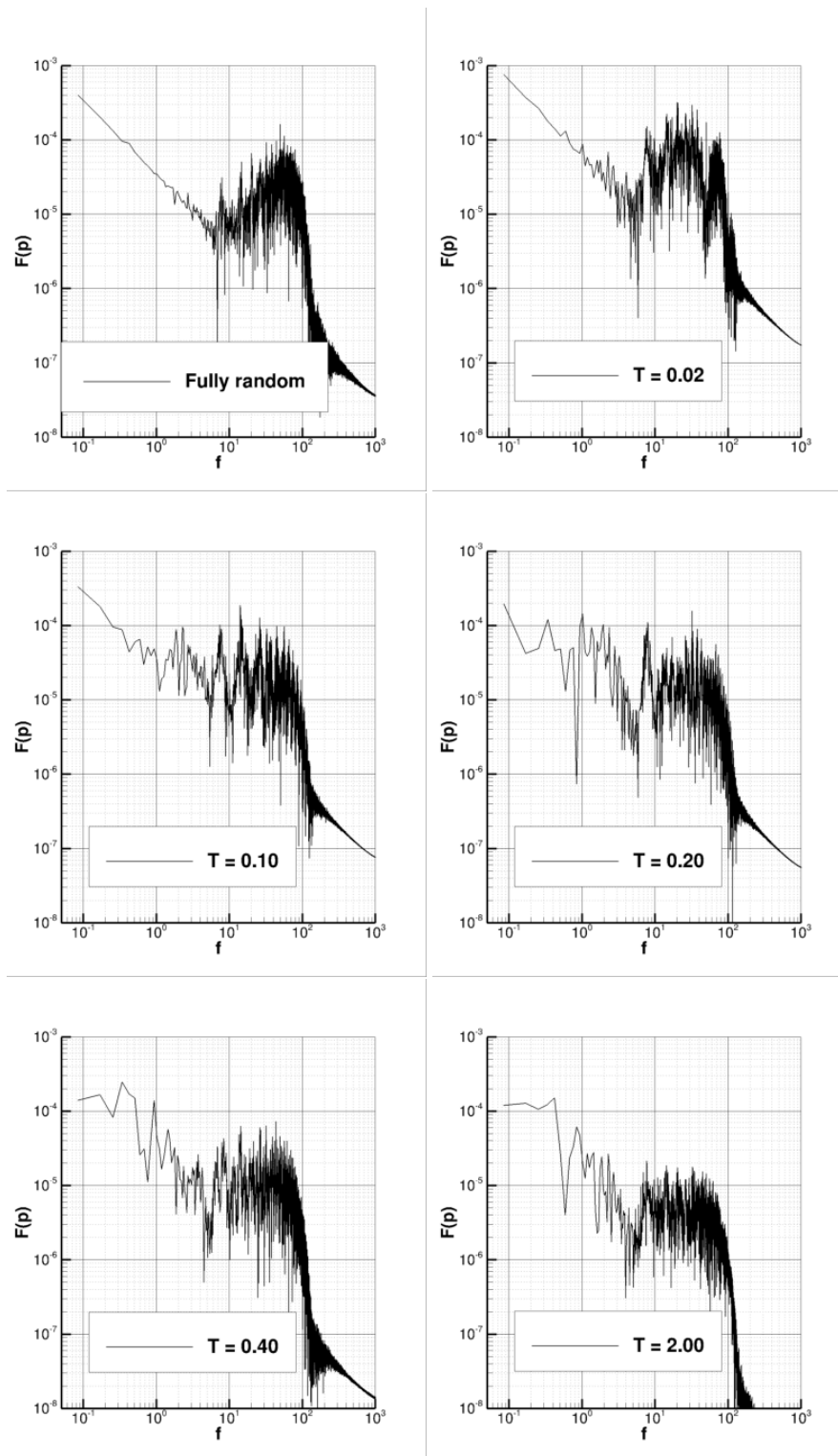
Figure 9: Fourier transform of head pressure for random perturbations with different correlation times

[3] S Gallier and M Plaud. A model for solid propellant burning fluctuations using mesoscale simulations. In *7^{t}h EUROPEAN CONFERENCE FOR AERONAUTICS AND SPACE SCIENCES (EUCASS)*, 2017.

[4] GA Gerolymos, D Sénéchal, and I Vallet. Very-high-order weno schemes. *Journal of Computational Physics*, 228(23):8481–8524, 2009.
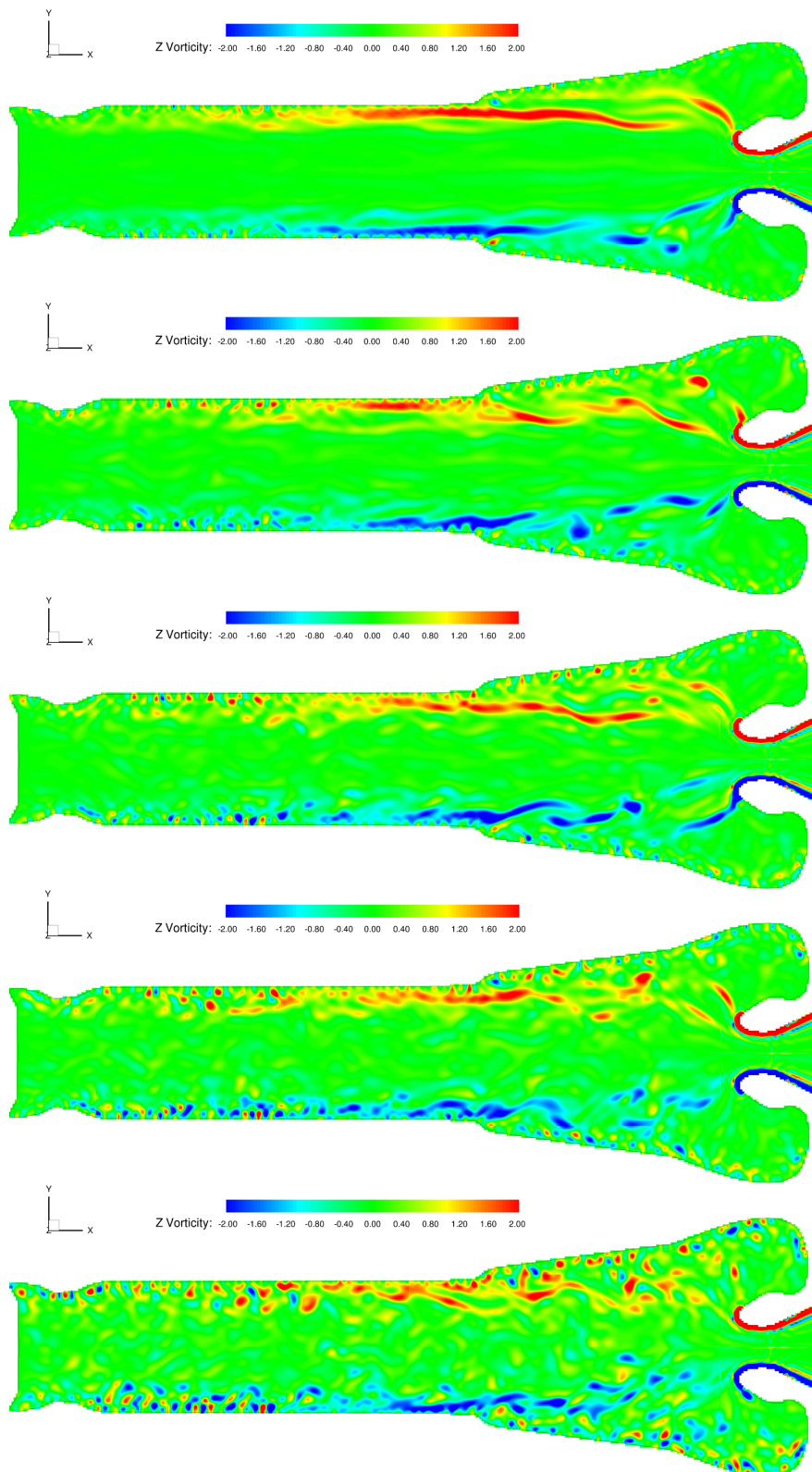
Figure 10: Z component of vorticity for random perturbations with different correlation times and amplitude 50%. Top to bottom: correlation time $T = 0.02$, $T = 0.1$, $T = 0.2$, $T = 0.4$ and $T = 2$..

[5] Guang-Shan Jiang. *Efficient implementation of weighted ENO schemes*. Department of Mathematics, University of California, Los Angeles, 1995.
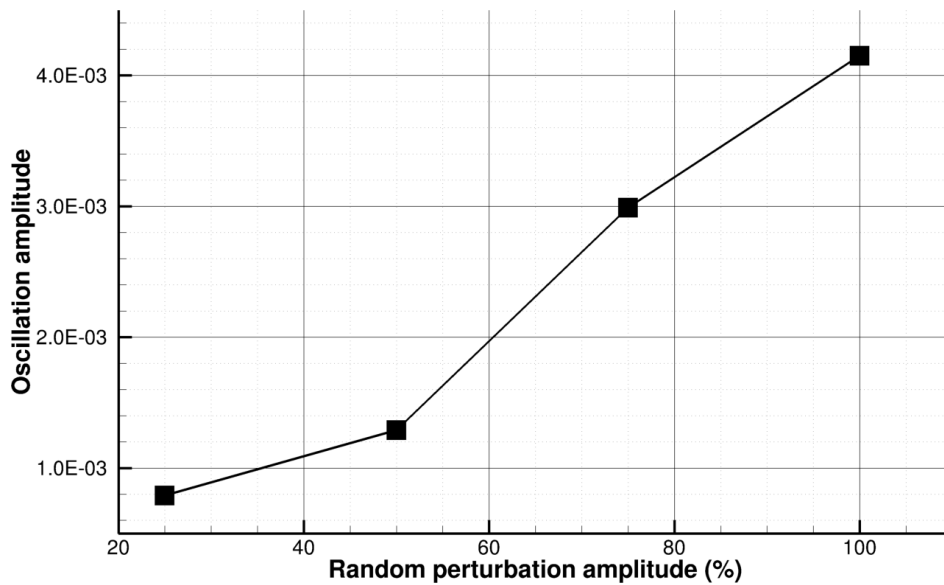
Figure 11: Head pressure oscillation amplitude as function of random perturbation amplitude for correlation time $T = 0.4$.
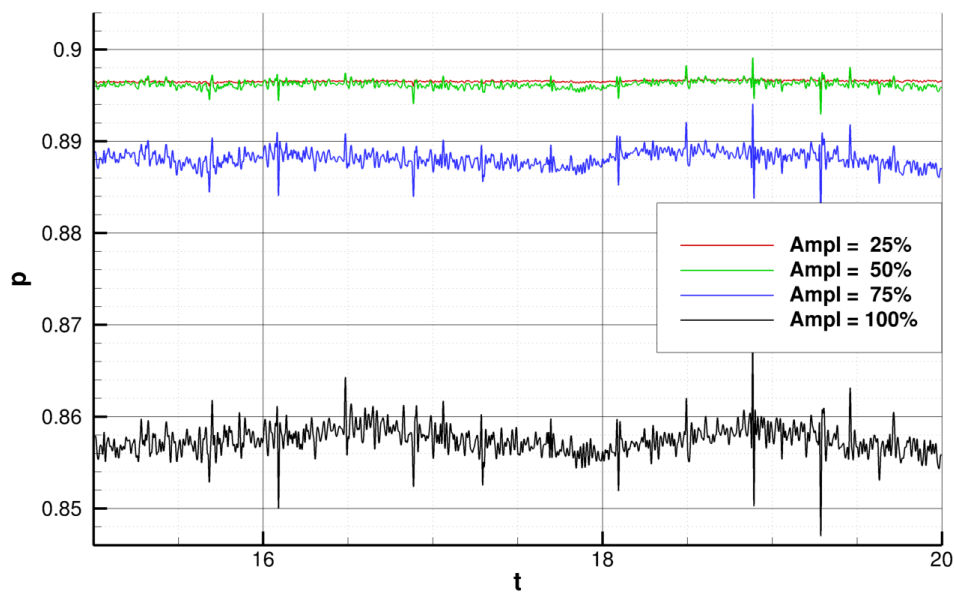

Figure 12: History of head pressure for random perturbations with correlation time $T = 0.4$ and various amplitudes.

[6] L Massa, TL Jackson, J Buckmaster, and F Najjar. Fluctuations above a burning heterogeneous propellant. *Journal of Fluid Mechanics*, 581:1–32, 2007.

[7] PR Spalart, WH Jou, M Strelets, and SR Allmaras. Comments on the feasibility of les for wings, and on a hybrid rans/les approach. 1st afosr int. In *Symp. Eng. Turb. Modelling and Measurements, May*, pages 24–26, 1997.

[8] Joseph L Steger and RF Warming. Flux vector splitting of the inviscid gasdynamic equations with application to finite-difference methods. *Journal of computational physics*, 40(2):263–293, 1981.

[9] H Werner and H Wengle. Large-eddy simulation of turbulent flow over and around a cube in a plate channel. In *Turbulent shear flows 8*, pages 155–168. Springer, 1993.